SUPERRESOLUTION PARALLEL MRI

[1]*Ricardo Otazo,* [1]*Ramiro Jordan,* [2] *Fa-Hsuan Lin and* [1,3]*Stefan Posse*

[1]Electrical and Computer Engineering Department, University of New Mexico, Albuquerque, NM, USA
[2]Martinos Center for Biomedical Imaging, Massachusetts General Hospital, Charlestown, MA, USA
[3]Department of Psychiatry, University of New Mexico, Albuquerque, NM, USA

ABSTRACT

Parallel MRI reconstruction is formulated as a superresolution problem using coil sensitivities acquired with higher spatial resolution than the actual image. Array coils with a large number of small elements that present very localized and highly modulated sensitivity functions will form an encoding basis to estimate high k-space components from limited k-space acquisitions. The method is proposed for spatial resolution enhancement of intrinsic low-resolution modalities such as spectroscopic imaging and functional MRI where the coil sensitivities are varying withing the image voxel.

Index Terms— MRI, parallel imaging, superresolution.

1. INTRODUCTION

Magnetic Resonance Imaging (MRI) methods involve imaging objects with high spatial frequency content in a limited amount of time. Conventional Fourier encoding, where the spatial frequency domain (k-space) of the object is sampled uniformly using a Cartesian grid, is very time consuming since only one k-space position is sampled at a time. Therefore, information over only a limited k-space range is usually available in practice due to time constraints. The lack of high spatial frequency information leads to limited spatial resolution and ringing when the Fourier transform is applied to reconstruct the image [1]. Constrained image reconstruction techniques [2] have been used to achieve superresolution, this is to estimate high frequency components without actually measuring them using prior information. For example, the finite spatial support of an image has been used to perform extrapolation of k-space [3]. Parametric modeling using a high resolution reference and a series of low resolution acquisitions [4] has also been employed for superresolution reconstruction.

Parallel MRI (PMRI) [5, 6] has been introduced as a method to accelerate the encoding process using an array of receiver coils with spatially-varying spatial sensitivities. The knowledge of coil sensitivities allows for reconstruction of sub-sampled data provided by the array. This acceleration could be used to increase k-space coverage in order to obtain a reconstructed image with higher spatial resolution. However, a larger coverage of k-space in the acquisition will produce a SNR loss that can be prohibitive for certain MRI modalities such as spectroscopic imaging. Therefore, superresolution reconstruction is advantageous to restore high spatial frequency components without reducing the SNR of the low resolution acquisition.

This work presents a novel method to achieve superresolution MRI reconstruction using parallel imaging concepts. Additional information to increase the spatial resolution of the acquisition is obtained from coil sensitivities acquired with higher spatial resolution. The technique is proposed for spatial resolution enhancement of inherent low-resolution MRI modalities such as spectroscopic imaging, which is constrained by low SNR, and functional MRI, which is constrained by the need for high temporal resolution.

2. METHODS

2.1. Superresolution Parallel MRI

The idea behind superresolution parallel MRI is to use coil sensitivity maps with higher spatial resolution to estimate high spatial frequency components of the object function from limited k-space acquisitions provided by the array coil (**Fig. 1**). In other words, the method will transfer the high spatial resolution of the sensitivity profiles to the low spatial resolution acquisition.

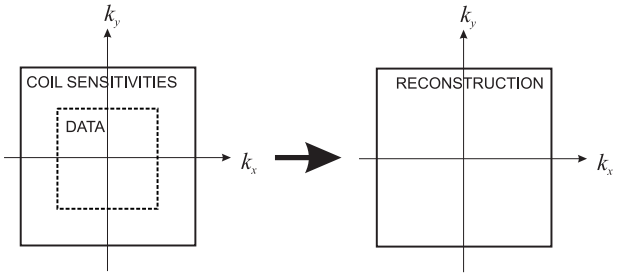

Fig. 1. Superresolution parallel MRI idea: transference of spatial resolution from the coil sensitivities to the acquisition.

This work was supported by National Institutes of Health Grants R01-HD040712, R01-NS037462, R01-EB000790-04, and R01 DA14178-01 and by the Mental Illness and Neuroscience Discovery (MIND) Institute.

The working hypothesis is that the coil sensitivities will provide extended k-space information. Even though this provides only limited k-space expansion for commercially available arrays with a small number of elements and therefore very smooth sensitivity functions, recently developed array designs with a large number of small elements will provide very localized information in the spatial domain that will increase k-space coverage of the sensitivity function [7].

The mathematical formulation of the method follows the description of parallel MRI reconstruction with a different sampling pattern. For superresolution parallel MRI, imaging data is acquired with limited k-space coverage and coil sensitivity data is acquired with a larger range of k-space values (**Fig. 1**). Both data sets are acquired at the Nyquist rate. In addition to the spatial encoding provided by the gradients, the signal acquired by each coil is sensitivity encoded and can be represented as:

$$Y_l(\mathbf{k}) = \int_{\mathbf{r}} s(\mathbf{r}) c_l(\mathbf{r}) e^{j2\pi \mathbf{k}\cdot\mathbf{r}} d\mathbf{r}, \;\; l = 1, 2, ..., N_c \; ; \quad (1)$$

where $\mathbf{r}$ is the position vector, $\mathbf{k} = \gamma \int_0^\tau \mathbf{G}(t)\, dt$ is the spatial frequency vector determined by the gradient vector $\mathbf{G}(t)$, $s(\mathbf{r})$ is the object function, $c_l(\mathbf{r})$ is the complex-valued spatialy-varying coil sensitivity and N_c is the number of coils. Considering the discretization of the object function to N_r points (target resolution), and the acquisition of N_k k-space points, a discretized version of Eq. (1) is given by:

$$Y_{l,n} = \sum_{m=1}^{N_r} s\left[\mathbf{r}_m\right] c_l\left[\mathbf{r}_m\right] e^{j2\pi \mathbf{k}_n \cdot \mathbf{r}_m}, \quad (2)$$

where $n = 1, 2, ..., N_k$ is the k-space index, $m = 1, 2, ..., N_r$ is the object index and ($l = 1, 2, ..., N_c$) is the coil index. Note that if we sample at the Nyquist rate, the acquisition of low resolution images can be represented using $N_k < N_r$. This encoding equation can be expressed using a matrix formulation:

$$\mathbf{y} = \mathbf{E}\,\mathbf{s}, \quad (3)$$

where $\mathbf{y}$ is the observation vector ($N_k N_c \times 1$), $\mathbf{E}$ is the encoding matrix ($N_k N_c \times N_r$) and $\mathbf{r}$ is the object vector ($N_r \times 1$). The entries of the encoding matrix are given by the hydrid encoding basis $c_l(\mathbf{r}_m) e^{j2\pi \mathbf{k}_n \cdot \mathbf{r}_m}$. Note that the encoding equation provides a forward model to describe the acquisition of low resolution images (N_k k-space points). The solution to the inverse problem will provide an image with the resolution of the coil sensitivity maps (N_r k-space points).

A direct solution of the parallel imaging problem is computationally intensive. More computationally tractable solutions can be achieved using uniform sampling, where the full reconstruction can be modeled as a series of 1-D reconstructions. Assuming a 1-D model with uniform sampling of k-space, the dicretized signal received by each coil is represented as:

$$Y_{l,n} = \sum_{r=0}^{N_r - 1} s[r] c_l[r] e^{j2\pi n \Delta k\, r}, \quad (4)$$

where Δk is the Nyquist rate. To achieve superresolution reconstruction, the coil sensitivity maps consist of N_r points ($N_r > N_k$). This encoding equation can be expressed using the following matrix formulation:

$$\mathbf{Y}_l = \mathbf{U}^H \mathrm{diag}\left\{\mathbf{c}_l\right\} \mathbf{s}, \quad (5)$$

where $\mathbf{Y}_l$ is the the observation vector for each coil ($N_k \times 1$), the elements of $\mathbf{U}^H$ ($N_k \times N_r$) correspond to the exponential terms in Eq. (4), the $N_r \times N_r$ diagonal matrix diag $\{\mathbf{c}_l\}$ contains $\{c_l[r]\}$ in the main diagonal and $\mathbf{s}$ is the the object vector ($N_r \times 1$). The rows of $\mathbf{U}^H$ correspond to the columns of the DFT matrix operator, and are mutually orthogonal. However, due to limited sampling the columns of $\mathbf{U}^H$ are not longer orthogonal. In the case of 2D imaging and sub-sampling along two dimensions, the encoding equation can be represented as:

$$\mathbf{Y}_l = \left(\mathbf{U}^H \otimes \mathbf{P}^H\right) \mathrm{diag}\left\{\mathrm{vec}\left\{\mathbf{c}_l\right\}\right\} \mathbf{s}, \quad (6)$$

where $\mathbf{U}^H$ and $\mathbf{P}^H$ represent the sampling pattern along the two spatial dimensions and $\otimes$ refers to the Kronecker product. The full linear system is formed by concatenating the signals from each coil:

$$\begin{bmatrix} \mathbf{Y}_1 \\ \mathbf{Y}_2 \\ \vdots \\ \mathbf{Y}_{N_c} \end{bmatrix} = \begin{bmatrix} \left(\mathbf{U}^H \otimes \mathbf{P}^H\right) \mathrm{diag}\left\{\mathrm{vec}\left\{\mathbf{c}_1\right\}\right\} \\ \left(\mathbf{U}^H \otimes \mathbf{P}^H\right) \mathrm{diag}\left\{\mathrm{vec}\left\{\mathbf{c}_2\right\}\right\} \\ \vdots \\ \left(\mathbf{U}^H \otimes \mathbf{P}^H\right) \mathrm{diag}\left\{\mathrm{vec}\left\{\mathbf{c}_{N_c}\right\}\right\} \end{bmatrix} \mathbf{s}, \quad (7)$$

which is in the same form as Eq. (3). The linear system can be solved using the minimum variance least squares solution [8]:

$$\hat{s} = \left(\mathbf{E}^H \Psi^{-1} \mathbf{E}\right)^{-1} \mathbf{E}^H \Psi^{-1} \mathbf{y}. \quad (8)$$

where Ψ is the noise correlation matrix of the array coil and H is the Hermitian conjugate operator.

2.2. Point Spread Function (PSF)

Reconstruction from limited k-space data can be represented as the convolution of the true object function $s(\mathbf{r})$ with the point spread function of the reconstruction method $h(\mathbf{r})$ [1]:

$$\hat{s}(\mathbf{r}) = s(\mathbf{r}) * h(\mathbf{r}). \quad (9)$$

The properties of a linear reconstruction technique such as the one proposed here can be characterized using the PSF. The width of the main lobe represents the spatial resolution and the amplitude of the side lobes represents the level of contamination from adjacent voxels.

The PSF will be computed by reconstructing simulated data from a source point, e.g. $s(\mathbf{r}_0) = \delta(\mathbf{r}_0)$ where δ is the Dirac function and $\mathbf{r}_0$ is the position of the source point. Spatial resolution will be computed using the full width at half maximum (FWHM) of the main lobe of the resulting PSF.

2.3. Experiments

2.3.1. Measurements

Phantom and human brain data were acquired using a gradient-echo sequence with a 32-channel array coil at 3 Tesla [7]. Phantom data was acquired using a 128×128 spatial matrix and a field of view (FOV) of 240×240 mm^2, resulting in a spatial resolution of 3.5 mm^2. Human brain data was acquired using a 256×256 spatial matrix and a field of view (FOV) of 256×256 mm^2, resulting in a spatial resolution of 1 mm^2. Reconstruction of the high resolution multi-channel human brain data was performed using sum-of-squares combination [9] (**Fig. 2.c**).

2.3.2. High resolution coil sensitivity maps

Coil sensitivity information were estimated at the high spatial resolution of the acquisition. Sensitivity profiles were computed following the method presented by Pruessmann *et al.* [8]. Raw sensitivity maps were obtained dividing the image from each coil by the high resolution reconstruction. Finally, 3^{rd} order polynomial fitting was used to refine the maps.

2.3.3. Simulations

Simulated data were created using the high resolution sensitivity functions from the phantom data resulting in a data set with 32 channels. Simulation A: Multi-coil data was generated by multiplying a numerical phantom (**Fig. 3**) with the sensitivity profiles and adding Gaussian noise. Simulation B: Multi-coil spectroscopic imaging data was generated in the same way by simulating a phantom with compartments for water (4.7 ppm), NAA (2.0 ppm) and lipids (1.3 and 2.0 ppm). Spectroscopic imaging data consists of spatial and spectral information, e.g. for each pixel we have a spectrum. The lipid resonances were located in a ring at the periphery of the phantom and assuming an concentration of 5 to 1 respect to NAA (**Fig. 4**). Images were obtained by spectral integration around the peak of interest.

2.3.4. Data reconstruction

Low resolution data was obtained from the central 32x32 k-space matrix. Reconstruction of the low resolution multi-coil data was performed using sum-of-squares [9]. For comparison purposes, this result was interpolated to a 128x128 spatial grid using Fourier interpolation (zero-padding). Superresolution parallel MRI reconstruction was applied to the low resolution data using the high resolution coil sensitivity maps.

3. RESULTS

The proposed method for superresolution using parallel MRI reconstruction highly improved the spatial response of conventional Fourier reconstruction, presenting a PSF with reduced main lobe width and highly attenuated side lobes (**Fig. 2.a**). The FWHM of the main lobe has been reduced from 5.0 to 1.63 poits which indicates a gain in spatial resolution by a factor of 3.

Superresolution PMRI reconstruction of the numerical phantom (**Fig. 2.b**) and the human brain (**Fig. 2.c**) also presented an improved spatial response with better defined spatial patterns and edges, and reduced ringing in the reconstructed image. For the human brain data set we can see improved tissue layers (arrows in **Fig. 2.c**).

Lipid contamination due to the side lobes of the PSF were also highly reduced in the simulated spectroscopic imaging experiment (**Fig. 4**). The NAA image presents a improved reconstruction using the superresolution PMRI approach.

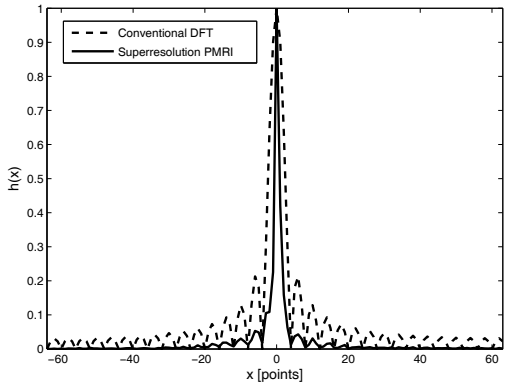

(a) Point spread function.

(b) Numerical phantom reconstruction.

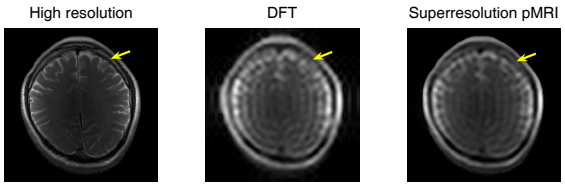

(c) Human brain reconstruction.

Fig. 2. (a) PSF comparison for superresolution pMRI and conventional Fourier reconstruction along the x dimension. Reconstruction results for: (b) simulated phantom and (c) in vivo experiment.

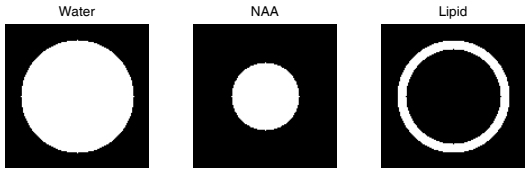

(a) Simulated metabolite compartments.

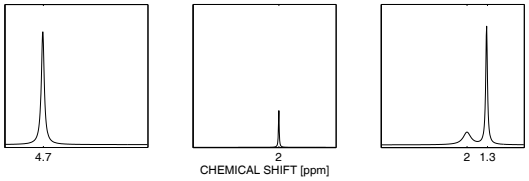

(b) Simulated spectra.

(c) Reconstructed images for 2.0 ppm.

Fig. 3. Simulated spectroscopic imaging experiment. (a) Spatial distribution of water, NAA and lipid inside the simulated phantom. (b) Corresponding spectral peaks. (c) NAA and lipid images at 2.0 ppm. Note that ringing and lipid contamination are highly reduced when using superresolution PMRI.

4. DISCUSSION

This work demonstrated feasibility of superresolution parallel MRI reconstruction for low spatial resolution imaging where the coil sensitivities are varying within the image voxel. High k-space components were estimated from limited k-space acquisitions using high resolution coil sensitivities as prior information. The method transferred the high resolution of the coil sensitivities to the image acquired with lower resolution. The array coil with 32 elements at 3 Tesla provided very localized and highly modulated coil sensitivity profiles which translated to larger coverage of k-space. However, small surface coils present SNR reduction in central zones that could limit the spatial coverage of the method. We are in the process of implementing the technique using a 32-channel array coil at 7 Tesla which will provide higher sensitivity and stronger spatial modulation of the sensitivity functions [10]. Future work also includes the application of the technique to human brain spectrospic imaging data and functional MRI, where the acquisition of a high resolution coil sensitivity information does not represent a time penalty due to the large number of repetitions in the experiment.

5. ACKNOWLEDGEMENTS

We thank Graham G. Wiggins and Lawrence Wald for the 32-channel array coil availability.

6. REFERENCES

[1] Z-P. Liang and P. Lauterbur, *Principles of Magnetic Resonance Imaging: A Signal Processing Perspective*, IEEE Series in Biomedical Engineering, 2000.

[2] Z-P. Liang, F. Boada, T. Constable, E.M. Haacke, P.C. Lauterbur, and M.R. Smith, "Constrained Reconstruction Methods in MR Imaging," *Reviews of Magnetic Resonance in Medicine*, vol. 4, pp. 67–185, 1992.

[3] S. Plevritis and A. Macovski, "Spectral extrapolation of spatially bounded images," *IEEE Transactions on Medical Imaging*, vol. 14, no. 3, pp. 487–497, 1995.

[4] Z-P. Liang and P.C. Lauterbur, "A generalized series approach to MR spectroscopic imaging," *IEEE Transactions on Medical Imaging*, vol. 10, no. 2, pp. 132–137, 1991.

[5] D.K. Sodickson and C.A. McKenzie, "A Generalized Approach to Parallel Magnetic Resonance Imaging," *Medical Physics*, vol. 28, no. 8, pp. 1629–1643, 2001.

[6] K.P. Pruessmann, "Encoding and Reconstruction in Parallel MRI.," *NMR in Biomedicine*, vol. 19, no. 3, pp. 288–299, 2006.

[7] G.C. Wiggins, C. Triantafyllou, A. Potthast, A. Reykowski, M. Nittka, and L.L. Wald, "32-Channel 3 Tesla Receive-Only Phased-Array Head Coil with Soccer-Ball Element Geometry," *Magnetic Resonance in Medicine*, vol. 56, no. 1, pp. 216–223, 2006.

[8] K.P. Pruessmann, M. Weiger, M.B. Scheidegger, and P. Boesiger, "SENSE: Sensitivity Encoding for Fast MRI.," *Magnetic Resonance in Medicine*, vol. 42, no. 5, pp. 952–962, 1999.

[9] D. Erdogmus, R. Yan, E.G. Larsson, J.C. Principe, and J.R. Fitzsimmons, "Image Construction Methods for Phased Array Magnetic Resonance Imaging," *Journal of Magnetic Resonance Imaging*, vol. 20, no. 2, pp. 306–314, 2004.

[10] F. Wiesinger, P.F. Van de Moortele, G. Adriany, N. De Zanche, K. Ugurbil, and K.P. Pruessmann, "Parallel Imaging Performance as a Function of Field Strength - An Experimental Investigation Using Electrodynamic Scaling," *Magnetic Resonance in Medicine*, vol. 52, no. 5, pp. 953–964, 2004.